engineering proceedings

MDPI

Proceeding Paper

Parametric Optimization of Solar Air Heaters Having Hemispherical Protrusion Roughness in the V-Notch Pattern on the Absorber Plate: A Metaheuristics Optimization Approach †

Premchand Kumar Mahto [1,2,*] and Balaram Kundu [2,*]

[1] Department of Mechanical Engineering, Sikkim Manipal Institute of Technology, Sikkim Manipal University, Majhitar 737136, Sikkim, India
[2] Department of Mechanical Engineering, Jadavpur University, Kolkata 700032, West Bengal, India
* Correspondence: prem4es@gmail.com (P.K.M.); bkundu@mech.net.in (B.K.)
† Presented at the International Conference on Recent Advances in Science and Engineering, Dubai, United Arab Emirates, 4–5 October 2023.

Abstract: Artificial roughness in the form of protrusions has become a popular technique to improve the thermohydraulic performance of SAHs. So, utmost attention should also be given to determining the suitable parametric values that directly affect the performance of SAHs. Hence, in this work, an attempt has been made to optimize the performance of solar air heaters having hemispherical protrusion roughness in a V-notch pattern on an absorber plate using two different metaheuristic optimization algorithms, i.e., the grey wolf optimization (GWO) algorithm and the dragonfly (DA) algorithm. This study makes use of the correlation equations for the friction factor (f_f) and Nusselt number (Nu), which were developed after conducting the experiments. Four independent parameters, namely the Reynolds number (Re = 3600–21,700), relative protrusion height (e_p/D_h = 0.027–0.069), relative pitch (p/e_p = 6–14), and attack angle (α_a = 15°–75°), were considered to obtain the optimal values of Nu and f_f. In single-objective optimization, the maximization of Nu and the minimization of f_f are two objective functions. The GWO has delivered the best solutions for both objectives with a faster computational rate and less variation. A convergence curve and box plot validated these findings. The maximum value of Nu was found to be 144.567, corresponding to Re = 21,700, e_p/D_h = 0.07, p/e_p = 8.54, and $\alpha_a = 75^0$, and the minimum value of f_f was found to be 0.012, corresponding to Re = 21,700, e_p/D_h = 0.03, p/e_p = 14, and α_a = 15°. Pareto multi-objective optimization provides compromised solutions that provide flexibility to the decision maker in selecting a parametric setting.

Keywords: metaheuristic; optimization; solar air heater; hemispherical protrusion; Nusselt number; friction factor

Citation: Mahto, P.K.; Kundu, B. Parametric Optimization of Solar Air Heaters Having Hemispherical Protrusion Roughness in the V-Notch Pattern on the Absorber Plate: A Metaheuristics Optimization Approach. *Eng. Proc.* **2023**, *59*, 183. https://doi.org/10.3390/engproc2023059183

Academic Editors: Nithesh Naik, Rajiv Selvam, Pavan Hiremath, Suhas Kowshik CS and Ritesh Ramakrishna Bhat

Published: 18 January 2024

1. Introduction

In recent years, the demand for electricity requirements has increased drastically due to technological enhancement, population growth, and an improvement in the standards of living [1]. So, people are searching for alternative energy resources, i.e., solar, wind, and hydro, to fulfill the energy demand. Solar thermal energy can be used for various purposes, like air heating, water heating, drying, etc. A solar air heater heats ambient air by trapping solar thermal energy, but it has low thermal performance due to the formation of a laminar sub-layer over a heated absorber plate [2]. Various techniques, such as packed beds, ribs, fins, dimples, and protrusion, are used to improve the thermohydraulic performance by breaking the laminar sub-layer [3–5]. Artificial roughness, such as dimples and protrusions, has become the most popular technique [6–9]. Employing roughness in the absorber plate increases the convective heat transfer by breaking the laminar sub-layer and developing a secondary flow; however, it also increases the pressure drop due to friction. Hence, it

becomes important to optimize the design parameters of protrusions to achieve high heat transfer rates with low friction losses [10].

Researchers have used various optimization techniques, such as ANN, SIPT, Taguchi, RMS, MCDM, AHP-TOPSIS, entropy–VIKOR, etc., to design and model the influencing parameters of solar air heaters [11]. The conventional optimization techniques have a number of complications, such as the fact that they require large input parameters, large dimensions, long iterations, and specific designs for each problem, and they struggle to provide global solutions. Conversely, metaheuristic optimization algorithms are simple, robust, flexible, scalable, and easy in execution for solving complex and real-world problems [12–14]. Many metaheuristic algorithms, such as PSO, GA, TLBO, ETLBO, and ABC, etc., have been applied in this search area [15]. From the above-cited literature, the following research gaps are identified:

a. Very few swarm intelligence-based metaheuristic optimization algorithms have been explored for the parametric optimization of solar air heaters with protrusion roughness in the form of V-notch patterns.
b. No study has been reported using the GWO and DA metaheuristic optimization algorithms.

So, to fill the above research gaps, this research work presents the single- and multi-objective parametric optimization of solar air heaters with protrusion roughness in the form of V-notch patterns using the GWO and DA metaheuristic optimization algorithms.

2. Materials and Methods

2.1. Test Rig

An experimental test rig was designed, fabricated, and tested at Sikkim Manipal Institute of Technology, Sikkim, India, as per the ASHRAE [16] standard. The rectangular solar collector was made of plywood, having an entry section length of 800 mm, a test section length of 1000 mm, and an exit section length of 400 mm. The cross-section dimension of the duct was 330 × 30 mm, with a pertaining aspect ratio of 11. A pictorial sketch of the test rig is shown in Figure 1. The absorber plate of the solar collector was made of aluminum, having a 1000 mm length, 330 mm width, and 0.4 mm thickness. Hemispherical protrusions in the absorber plates, as shown in Figure 2, have been prepared with the help of 5 sets of punch and die. A heat flux of 1000 W/m^2 was provided using halogen lamps. The intensity of heat flux was measured and controlled using a pyranometer and an auto-transformer, respectively. A centrifugal blower was connected to the exit section to ensure a flow of air through the duct. The airflow was metered with the help of a regulating valve. A digital anemometer was employed to measure the airflow velocity. A total of twelve J-type thermocouples were employed to measure the temperature. A digital micrometer was employed to measure the pressure drop. All sets of these experiments were conducted in steady-state conditions. Four protrusion roughness parameters, namely relative pitch (p/e_p), relative height (e_p/D_h), attack angle (α_p), and Reynolds number (Re), as flow parameters were taken into account for conducting this investigation. The range of the roughness and flow parameters are provided in Table 1.

Table 1. Roughness and flow parameters.

Sl. Nos.	Parameter	Range
1	Relative height of roughness (e_p/D_h)	0.027–0.069
2	Relative pitch of roughness (p/e_p)	6–14
3	Attack angle (α_a)	15°–75°
4	Reynolds Number (Re)	3600–21,700

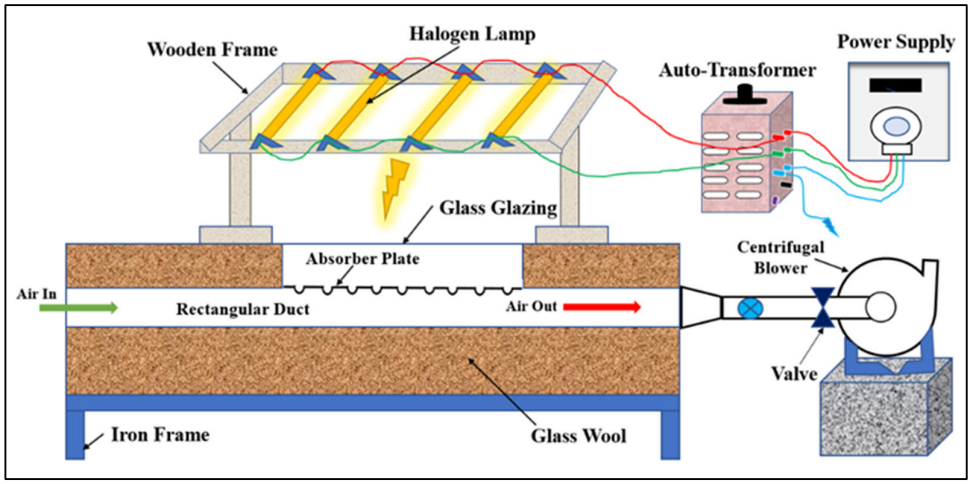

Figure 1. Schematic diagram of the test rig.

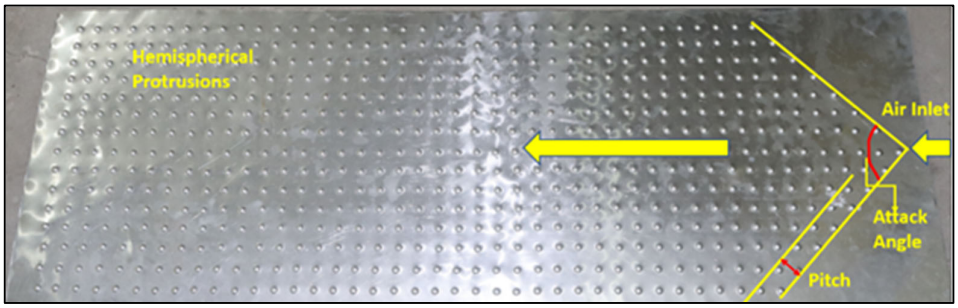

Figure 2. Absorber plate.

2.2. Metaheuristic Optimization

The conventional optimization methods have several problems, such as randomly initializing, problem-specific, large input parameters, large dimensions, poor convergence, long iterations, local optima, and struggling to provide global solutions. On the other hand, metaheuristic optimization has advanced significantly in the last three decades due to its four major features, i.e., simplicity, flexibility, derivation-free mechanism, and local optima avoidance. Favoring the qualities of metaheuristic optimization methodologies, two swarm intelligence-based metaheuristic algorithms, i.e., the grey wolf optimization algorithm (GWO) and the dragonfly optimization algorithm (DA), have been selected to execute single- and multi-objective optimization of the system and flow parameter of the aforesaid solar air heater. A detailed motivation and mathematical mode of the GWO and DA methods are discussed below.

2.2.1. The Grey Wolf Optimization Algorithm (GWO)

Scientifically called *Canis lupus*, the grey wolf belongs to the *Canidae* family and is considered an apex predator in the food chain. A group of grey wolves consists of four social hierarchies. Group hunting is the main process of collecting their food. The GWO method is motivated by the social hierarchy and hunting techniques of the grey wolf and is mathematically modeled as follows [17]: Social hierarchy: GWO optimization is guided by alpha, supported by beta and delta, and followed by omega. Alpha is considered the first best solution, followed by beta and delta.

Encircling of prey: The encircling of prey is the first phase in the hunting process. The encircling of prey can be modeled as follows:

$$\vec{m} = \left| \vec{C} - \vec{X_p}(t) - \vec{X_w}(t) \right| \quad (1)$$

$$\vec{X_w}(t+1) = \left|\vec{X_p}(t) - \vec{k}\cdot\vec{m}\right| \quad (2)$$

$$\vec{k} = 2\vec{a}\cdot\vec{r_1} - \vec{a} \quad (3)$$

$$\vec{C} = 2 - \vec{r_2} \quad (4)$$

where t = current iteration; $\vec{k}$ and $\vec{m}$ = coefficient vectors; $\vec{X_p}$ = position vector of the prey; $\vec{X_w}$ = position vector of the grey wolf; $\vec{a}$ = linear decrease from 2 to 0; and r_1 and r_2 are random vectors (0, 1).

Hunting: the hunting model can be considered as follows:

$$\vec{m_\alpha} = \left|\vec{C_1} - \vec{X_\alpha} - \vec{X_w}\right|, \vec{m_\beta} = \left|\vec{C_1} - \vec{X_\beta} - \vec{X_w}\right|, \vec{m_\delta} = \left|\vec{C_1} - \vec{X_\delta} - \vec{X_w}\right| \quad (5)$$

$$\vec{X_1} = \vec{X_\alpha} - \vec{k_1}\cdot\vec{m_\alpha}, \vec{X_2} = \vec{X_\beta} - \vec{k_2}\cdot\vec{m_\beta}, \vec{X_3} = \vec{X_\delta} - \vec{k_3}\cdot\vec{m_\delta} \quad (6)$$

$$\vec{X_w}(t+1) = \frac{\vec{X_1} + \vec{X_2} + \vec{X_3}}{3} \quad (7)$$

Attacking (exploitation): In the mathematical model, as $\vec{a}$ linearly decreased from 2 to 0 in each search, $\vec{k}$ simultaneously decreases with $\vec{a}$. Once the random value of $\vec{k}$ lies between -1 and 1, the subsequent location of the search agent lies between the present location and the location of the prey.

Exploration: The global search in all the possible regions comes under the exploration phase, and it is carried out once the results are stuck in their local optima. When the value of $\vec{k} > 1$, or $\vec{k} < -1$, the search agent diverges from the prey, and if $\vec{k} < 1$, the search agent converges to the prey and finally comes up with their final solutions. A flow diagram of the GWO algorithm, as discussed, is presented in Figure 3.

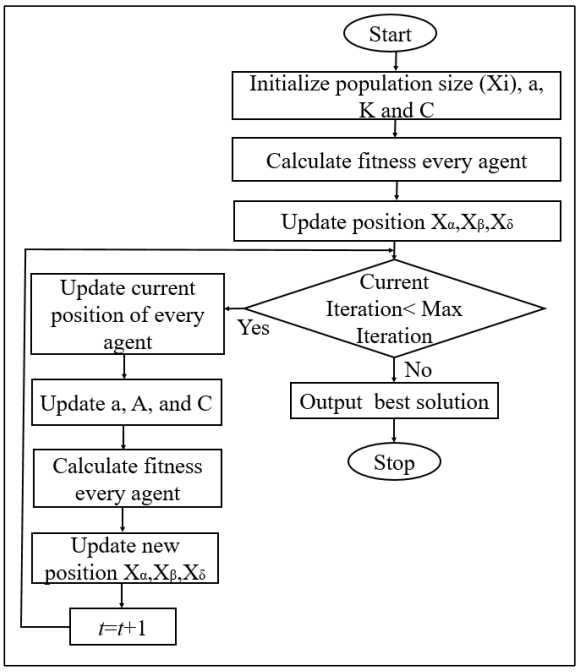

Figure 3. Flow chart of the GWO algorithm.

2.2.2. The Dragonfly Algorithm (DA)

Scientifically called *Odonata*, dragonflies are an insect with more than 3000 varieties in the world. The DA algorithm is inspired by the swarming behavior of dragonflies and

consists of two types, i.e., static and dynamic. Static behavior is considered under the exploration phase, in which a group of dragonflies fly around different locations. A large number of dragonflies move in specific directions in search of food, which is considered under the exploitation phase of the metaheuristic algorithm. To mimic the flying motions of dragonfly separation motion (S_i), alignment motion (A_i), cohesion motion (C_i), attraction towards food (F_i), and distraction from the predator (P_i), they can be mathematically modeled as follows [18]:

$$\text{Separation}: \ S_i = -\sum_{j=1}^{n} X - X_j \tag{8}$$

$$\text{Alignment}: \ A_i = \frac{\sum_{j=1}^{n} V_j}{n} \tag{9}$$

$$\text{Cohesion}: \ C_i = \frac{\sum_{j=1}^{n} X_j}{n} - X \tag{10}$$

$$\text{Attraction towards food}: \ F_i = X^+ - X \tag{11}$$

$$\text{Distraction from predators}: \ P_i = X^- + X \tag{12}$$

where X is the location of the individual; X_j is the location of the j^{th} dragonfly; n is the total number of neighboring individuals; X^+ is the position of the food; and X^- is the predator's position. The step vector (ΔX) and location vector (X) are two major parameters to update the current location and are calculated using the following equations:

$$\Delta X_{(t+1)} = (sS_i + aA_i + cC_i + fF_i + pP_i) + \omega \nabla X_t \tag{13}$$

$$X_{(t+1)} = X_t + \Delta X_{(t+1)} \tag{14}$$

where s, a, c, *f*, and p are the weights of each motion; ω is the inertia weight; t denotes the iteration number; and t + 1 is the current iteration. A flow diagram of the DA algorithm, as discussed above, is provided in Figure 4.

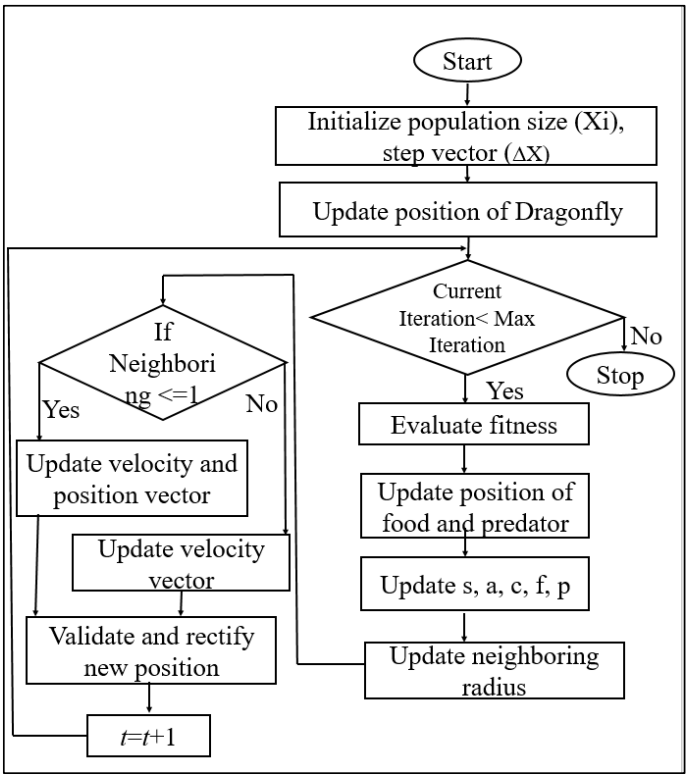

Figure 4. Flow chart of the DA algorithm.

3. Results and Discussion

3.1. Experimental Findings and Correlations

The experimental results showed an improvement in Nusselt number by employing hemispherical protrusions in V-notch patterns on the absorber plate. On the other hand, friction losses also increase, causing an increase in pumping power consumption. So, it is necessary to develop some correlations between dependent and independent parameters. The Nusselt number and friction factor are two major dependent parameters that are affected by independent parameters such as the Reynolds number, relative pitch, relative roughness height, and attack angle. The functional relation can be written as follows:

$$\mathrm{Nu} = f\ (\mathrm{Re}, \mathrm{e_p}/\mathrm{D_h}, \mathrm{p}/\mathrm{e_p}, \alpha_a) \tag{15}$$

$$f_f = f\ (\mathrm{Re}, \mathrm{e_p}/\mathrm{D_h}, \mathrm{p}/\mathrm{e_p}, \alpha_a) \tag{16}$$

A regression analysis has been conducted to develop the correlation for Nusselt number and friction factor, which are presented in Equations (17) and (18), respectively:

$$\mathrm{Nu} = 1.1513 \times 10^{-5}\mathrm{Re}^{0.0709}\left(\frac{\mathrm{e_p}}{\mathrm{D_h}}\right)^{0.2967}\left(\frac{\mathrm{p}}{\mathrm{e_p}}\right)^{6.7298}\left(\frac{\alpha_a}{45}\right)^{0.1482}\exp\left(0.0214 \times \ln\left(\frac{\mathrm{e_p}}{\mathrm{D_h}}\right)^2\right) \exp\left(-1.5693 \times \ln\left(\frac{\mathrm{p}}{\mathrm{e_p}}\right)^2\right)\exp\left(0.0032 \times \ln\left(\frac{\alpha_a}{45}\right)^2\right) \tag{17}$$

$$f_f = 4.39 \times 10^{-4}\mathrm{Re}^{-0.2842}\left(\frac{\mathrm{e_p}}{\mathrm{D_h}}\right)^{-1.9766}\left(\frac{\mathrm{p}}{\mathrm{e_p}}\right)^{3.7294}\left(\frac{\alpha_a}{45}\right)^{0.1296}\exp\left(-0.3381 \times \ln\left(\frac{\mathrm{e_p}}{\mathrm{D_h}}\right)^2\right) \exp\left(-0.8774 \times \ln\left(\frac{\mathrm{p}}{\mathrm{e_p}}\right)^2\right)\exp\left(-0.1549 \times \ln\left(\frac{\alpha_a}{45}\right)^2\right) \tag{18}$$

3.2. Single-Objective Optimization

The maximization of Nu and minimization of f_f are two objective functions for single-objective optimization. The correlation between Nu and f_f, as given in Equations (17) and (18), has been used to find the optimal parametric setting to fulfill the objective criterion. The search range of independent parameters is considered as per Table 1. The results of single-objective optimization are provided in Table 2. From the results table, it can be observed that the GWO algorithm outperforms the DA algorithm in solving both objectives. The maximum value of Nu was found to be 144.567, corresponding to Re = 21,700, $\mathrm{e_p}/\mathrm{D_h}$ = 0.07, $\mathrm{p}/\mathrm{e_p}$ = 8.54, and α_a = 75°, and the minimum value of f_f was found to be 0.012 with respect to Re = 21,700, $\mathrm{e_p}/\mathrm{D_h}$ = 0.03, $\mathrm{p}/\mathrm{e_p}$ = 14, and α_a = 15°. Also, the convergence curve, as shown in Figure 5, reveals that the GWO algorithm can achieve the best possible results with less computational effort and at a faster rate. The search results of Nu and f_f generated using both optimization algorithms are plotted in box plots and presented in Figures 6 and 7, respectively. It can be observed that the responses of Nu and f_f from the GWO algorithm are more consistent with fewer fluctuations than the DA algorithm, as most of the data reside near the mean value.

Table 2. Results of single-objective optimization.

Objective Function	Method	Mean Value	Standard Deviation	Optimal Output	Optimal Parameter Setting			
					Re	$\mathrm{e_p}/\mathrm{D_h}$	$\mathrm{p}/\mathrm{e_p}$	α_a
Nu	GWO	144.567	0	144.567	21,700	0.07	8.54	75
	DA	132.468	6.34	130.094	21,349.5	0.07	8.61	41.75
f_f	GWO	0.012	0	0.012	21,700	0.03	14	15
	DA	0.014	0.001	0.014	21,673.52	0.03	13.27	15

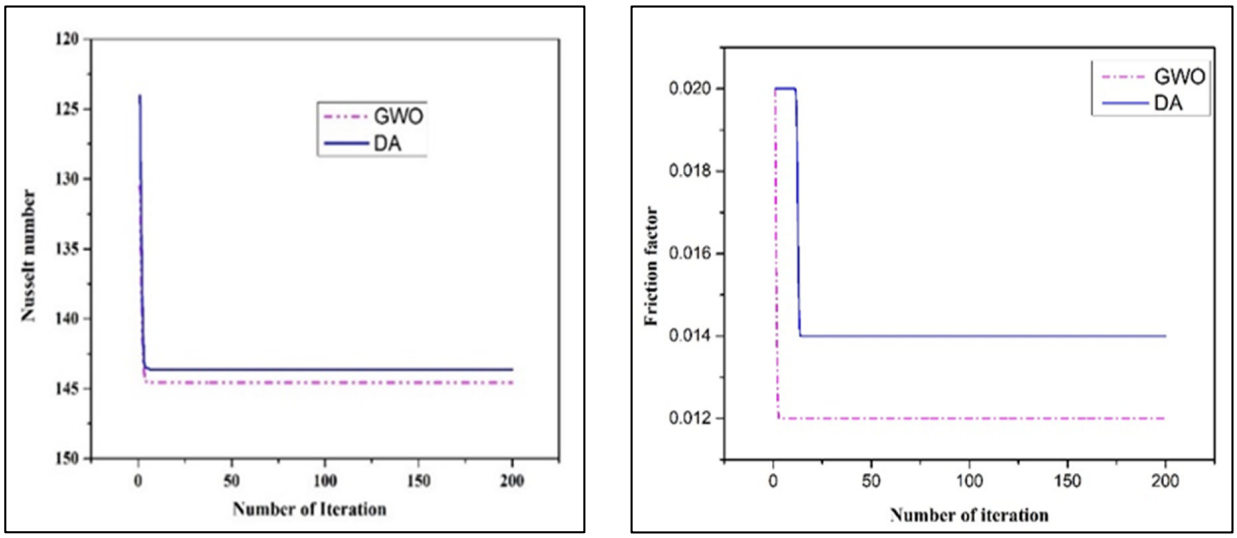

(**a**) (**b**)

Figure 5. Convergence curves for (**a**) the Nusselt number and (**b**) the friction factor.

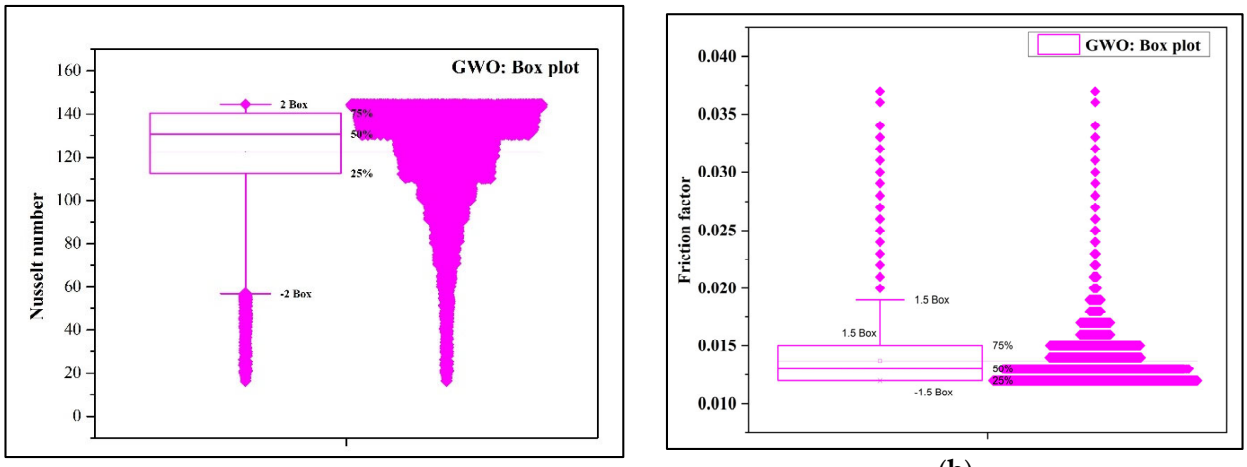

(**a**) (**b**)

Figure 6. GWO box plots for (**a**) the Nusselt number and (**b**) the friction factor.

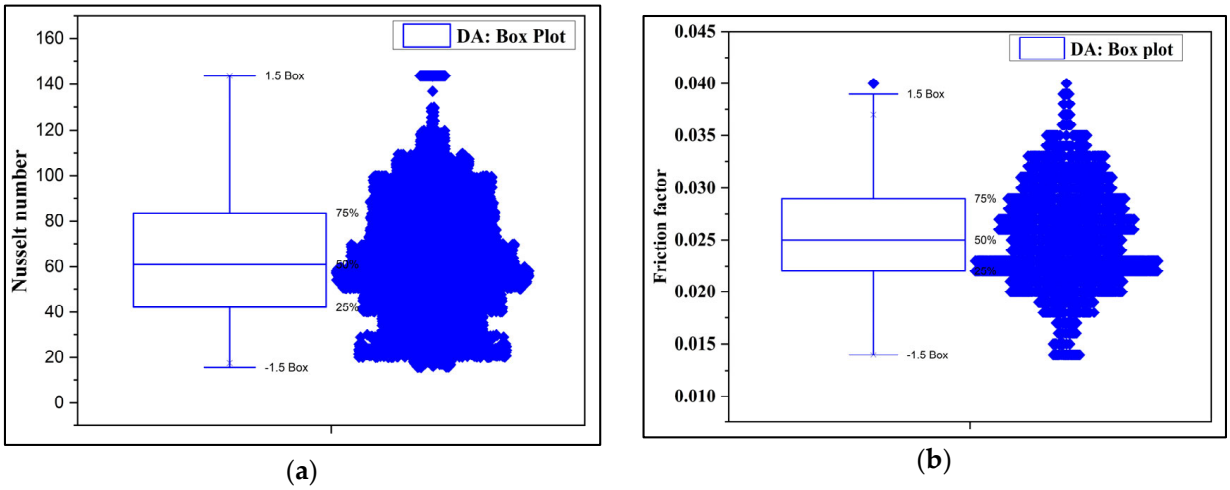

(**a**) (**b**)

Figure 7. DA box plots for (**a**) the Nusselt number and (**b**) the friction factor.

3.3. Multi-Objective Optimization

The optimal parametric setting of independent parameters obtained in single-objective optimization is different for the objective function, which is impractical in nature to employ at a given time. In this situation, metaheuristic algorithms are better suited than aggregation-based optimization techniques. In contrast, GWO and DA are used to solve both objectives at a given time and provide multiple compromised solutions. A total of 500 interns and 150 search agents were employed to find the optimal solutions. The Pareto front of compromised solutions generated using both metaheuristic algorithms is shown in Figure 8, and the optimal parametric setting for the upper and lower ranges of thermohydraulic performance index (THPi) is shown in Table 3. The Pareto front of GWO optimal solutions are more consistent and non-dominated, with less dissimilarity than DA. A compromised solution to the objective function can be found between the ranges. So, the decision makers have to decide about the selection of suitable parameters for obtaining optimal outputs. The comparison of the thermohydraulic performance index with related research articles is shown in Table 4. The results obtained showed an improvement in THPi than others.

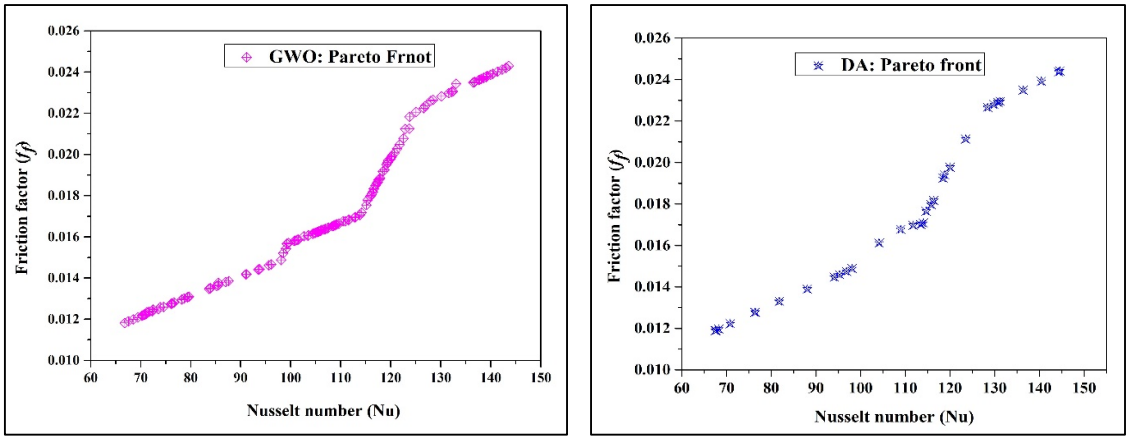

(**a**) (**b**)

Figure 8. The Pareto front of compromised solutions generated using (**a**) GWO and (**b**) DA.

Table 3. Results of multi-objective optimization.

Method	Range	Nu	f_f	THPi	Optimal Parameter Setting			
					Re	e_p/D_h	p/e_p	α_a
GWO	Upper	143.08	0.024	1.62	21,700	0.069	9.25	75
GWO	Lower	66.80	0.012	0.096	21,700	0.027	14	15
DA	Upper	144.55	0.024	1.63	21,700	0.069	8.58	74.97
DA	Lower	68.23	0.011	0.097	21,700	0.027	13.80	15

Table 4. Comparison of the THPi of the presented solar air heater with previous studies.

Sl. No.	Duct Type	Roughness Type	Maximum THPi
Xie et al. [19]	Rectangular	Dimple	1.2
Liu et al. [20]	Rectangular	Dimple	1.44
Chamoli et al. [21]	Rectangular	V-shaped rectangular perforated blocks	1.3
Present study	Rectangular	Protrusions in the V-notch pattern	GWO: 1.62 DA: 1.63

4. Conclusions

The parametric optimization of solar air heaters having hemispherical protrusion roughness in their V-notch patterns have been performed using two different metaheuristic optimization algorithms, i.e., GWO and DA. Both single- and multi-objective optimization have been presented, and the conclusions are as follows:

a. For maximizing Nu, GWO delivered the best solutions. The maximum value of Nu was found to be 144.567, corresponding to Re = 21,700, e_p/D_h = 0.07, p/e_p = 8.54, and $\alpha_a = 75^\circ$.
b. For minimizing f_f, GWO delivered the best solutions. The maximum value of f_f was found to be 0.012, corresponding to Re = 21,700, e_p/D_h = 0.03, p/e_p =14, and $\alpha_a = 15^\circ$.
c. GWO generated a consistent, non-dominated optimal solution under multi-objective optimization than DA.
d. Pareto multi-objective optimization provided compromised solutions that provided flexibility to the decision maker in selecting a parametric setting. The maximum THPi obtained using GWO and DA was 1.62 and 1.63, respectively.

Author Contributions: Conceptualization, P.K.M.; methodology, P.K.M.; software, P.K.M.; validation, P.K.M. and B.K.; formal analysis, P.K.M.; investigation, P.K.M.; resources, P.K.M.; data curation, P.K.M.; writing—original draft preparation, P.K.M.; writing—review and editing, B.K.; visualization, B.K.; supervision, B.K; project administration, B.K.; funding acquisition, P.K.M. All authors have read and agreed to the published version of the manuscript.

Funding: This research was funded by the TMA Pai faculty research grant at Sikkim Manipal University, India, Sikkim (TMA Pai faculty project: 6100/SMIT/R&D/PROJECT/06/2018).

Institutional Review Board Statement: Not applicable.

Informed Consent Statement: Not applicable.

Data Availability Statement: Data will be provided if any request is made.

Acknowledgments: The authors acknowledge the support provided by Sikkim Manipal Institute of Technology, Sikkim, India. The authors would also like to thank Gaurav Sapkota for his support.

Conflicts of Interest: The authors declare no conflicts of interest.

References

1. Zarco-Periñán, P.J.; Zarco-Soto, I.M.; Zarco-Soto, F.J. Influence of the population density of cities on energy consumption of their households. *Sustainability* **2021**, *13*, 7542. [CrossRef]
2. Reay, D.A. Heat transfer enhancement—A review of techniques and their possible impact on energy efficiency in the UK. *Heat Recovery Syst. CHP* **1991**, *11*, 1–40. [CrossRef]
3. Karsli, S. Performance analysis of new-design solar air collectors for drying applications. *Renew. Energy* **2007**, *32*, 1645–1660. [CrossRef]
4. Markam, B.; Maiti, S. Artificial enhancer for small-scale solar air heater—A comprehensive review. *Clean. Energy Syst.* **2022**, *4*, 100046. [CrossRef]
5. Yadav, A.K.; Choudhary, M.; Singh, A.P. Assessment of solar air heater performance using a variety of artificially roughened components. *Mater. Today Proc.* 2023, *in press*. [CrossRef]
6. Kumar, R.; Sharma, A.; Goel, V.; Sharma, R.; Sethi, M.; Tyagi, V.V. An experimental investigation of new roughness patterns (dimples with alternative protrusions) for the performance enhancement of solar air heater. *Renew. Energy* **2023**, *211*, 964–974. [CrossRef]
7. Kumar, V. Nusselt number and friction factor correlations of three sides concave dimple roughened solar air heater. *Renew. Energy* **2019**, *135*, 355–377. [CrossRef]
8. Rao, Y.; Li, B.; Feng, Y. Heat transfer of turbulent flow over surfaces with spherical dimples and teardrop dimples. *Exp. Therm. Fluid Sci.* **2015**, *61*, 201–209. [CrossRef]
9. Sethi, M.; Thakur, N.S. Correlations for solar air heater duct with dimpled shape roughness elements on absorber plate. *Sol. Energy* **2012**, *86*, 2852–2861. [CrossRef]
10. Deo, N.S.; Chander, S.; Saini, J.S. Performance analysis of solar air heater duct roughened with multigap V-down ribs combined with staggered ribs. *Renew. Energy* **2016**, *91*, 484–500. [CrossRef]

11. Elsheikh, A.H.; Abd Elaziz, M. Review on applications of particle swarm optimization in solar energy systems. *Int. J. Environ. Sci. Technol.* **2019**, *16*, 1159–1170. [CrossRef]
12. Madić, M.; Marković, D.; Radovanović, M. Comparison of meta-heuristic algorithms for solving machining optimization problems. *Facta Univ.-Ser. Mech. Eng.* **2013**, *11*, 29–44.
13. SS, V.C.; HS, A. Nature inspired meta heuristic algorithms for optimization problems. *Computing* **2022**, *104*, 251–269. [CrossRef]
14. Abdel-Basset, M.; Abdel-Fatah, L.; Sangaiah, A.K. Metaheuristic algorithms: A comprehensive review. In *Intelligent Data-Centric Systems, Computational Intelligence for Multimedia Big Data on the Cloud with Engineering Applications*; Sangaiah, A.K., Sheng, M., Zhang, Z., Eds.; Academic Press: Cambridge, MA, USA, 2018; pp. 185–231. [CrossRef]
15. Niyonteze, J.D.D.; Zou, F.; Asemota, G.N.O.; Nsengiyumva, W.; Hagumimana, N.; Huang, L.; Nduwamungu, A.; Bimenyimana, S. Applications of Metaheuristic Algorithms in Solar Air Heater Optimization: A Review of Recent Trends and Future Prospects. *Int. J. Photoenergy* **2021**, *2021*, 6672579. [CrossRef]
16. *ANSI/ASHRAE 93-2003*; Method of Testing to Determine the Thermal Performance of Solar Collectors. American Society of Heating, Refrigeration and Air Conditioning Engineers: Atlanta, GA, USA, 2003.
17. Mirjalili, S.; Mirjalili, S.M.; Lewis, A. Grey wolf optimizer. *Adv. Eng. Softw.* **2014**, *69*, 46–61. [CrossRef]
18. Mirjalili, S. Dragonfly algorithm: A new meta-heuristic optimization technique for solving single-objective, discrete, and multi-objective problems. *Neural Comput. Appl.* **2016**, *27*, 1053–1073. [CrossRef]
19. Xie, G.; Liu, J.; Ligrani, P.M.; Zhang, W. Numerical analysis of flow structure and heat transfer characteristics in square channels with different internal-protruded dimple geometrics. *Int. J. Heat Mass Transf.* **2013**, *67*, 81–97. [CrossRef]
20. Liu, J.; Song, Y.; Xie, G.; Sunden, B. Numerical modeling flow and heat transfer in dimpled cooling channels with secondary hemispherical protrusions. *Energy* **2015**, *79*, 1–19. [CrossRef]
21. Chamoli, S.; Thakur, N.S. Heat transfer enhancement in solar air heater with V-shaped perforated baffles. *J. Renew. Sustain. Energy* **2013**, *5*, 023122. [CrossRef]